Surface structure and structural point defects of liquid and amorphous aluminosilicate nanoparticles

2008 J. Phys.: Condens. Matter 20 265005

(http://iopscience.iop.org/0953-8984/20/26/265005)

J. Phys.: Condens. Matter **20** (2008) 265005 (9pp) doi:10.1088/0953-8984/20/26/265005

Surface structure and structural point defects of liquid and amorphous aluminosilicate nanoparticles

Nguyen Ngoc Linh and Vo Van Hoang

Department of Physics, Institute of Technology, National University of HoChiMinh City, 268 Ly Thuong Kiet Street, District 10, HoChiMinh City, Vietnam

E-mail: ngoclinh84phys@yahoo.com

Received 28 November 2007, in final form 28 April 2008
Published 22 May 2008
Online at stacks.iop.org/JPhysCM/20/265005

Abstract

The surface structure of liquid and amorphous aluminosilicate nanoparticles of composition $Al_2O_3{\cdot}2SiO_2$ has been investigated in a model of different sizes ranging from 2.0 to 5.0 nm with the Born–Mayer type pair potential under non-periodic boundary conditions. Models have been obtained by cooling from the melts at a constant density of 2.6 g cm^{-3} via molecular dynamics (MD) simulation. The surface structure has been investigated via the coordination number, bond-angle distributions and structural point defects. Calculations show that surface effects on surface static and thermodynamic properties of models are significant according to the change in the number of Al atoms in the surface layers. Evolution of the local environment of oxygen in the surface shell of nanoparticles upon cooling from the melt toward the glassy state was also found and discussed. In addition, the nanosize dependence of the glass transition temperature was presented.

1. Introduction

Understanding structural properties at an atomic level of aluminosilicate ceramic materials is essential due to their important applications such as protective coatings, electronic packaging, porous materials, optical materials and fiber technology [1–5]. In particular, liquid and amorphous aluminosilicate nanoparticles have been under intensive investigations due to their technological importance, i.e. they have applications in drug storage and release, biomedicine, optics and electronics, or in the adsorption of arsenic in order to remove them from aqueous environments [6–8]. Moreover, aluminosilicate nanoparticles containing 9.0–20 nm mesopores were prepared for the cracking of very large hydrocarbons in the oil industry [9, 10]. Therefore, the microstructure of liquid and amorphous aluminosilicate nanoparticles has aroused great interest from both experiments and computer simulations. Indeed, the amorphous nanoparticulate aluminosilicate 3/2-mullite precursor has been synthesized, and the sols containing 2 nm particles of Q^3(3Al) silica species together with six-coordinated alumina were found, which suggested an allophane-like structure for the nanoparticles. These sols were characterized by small-angle x-ray scattering, dynamic light scattering, x-ray diffraction, ^{27}Al and ^{29}Si MAS nuclear magnetic resonance spectroscopy, and differential thermal analysis [11]. In addition, aluminosilicate nanoparticles have also been produced in the forms of powder, sol–gel and composite coating particles [12, 13]. Furthermore, a local description of zeolites versus aluminosilicate clusters was shown by force field calculations on extended systems and by *ab initio* quantum chemical calculations on ring structures. It reveals that the relation and energy content of neutral-framework silicates are determined by that of the smallest substructures [14]. In the applications mentioned above, however, the surfaces and interfaces of amorphous aluminosilicate layers have a major effect on their functionality. Therefore, it is also important to gain an understanding of the surface structure in terms of the local atomic arrangement.

As a subset of material properties, surface properties of aluminosilicate nanoparticles have an important role in their applications in practice. It was found that high surface-specific reactions result from the substitution of Si in the SiO_2 matrix, and it creates a native charge on the SiO_2 framework with an associated H^+ being bonded to a nearby oxygen atom to maintain the charge neutrality [15]. This

results in the formation of Brönsted acid protons as Al–OH–Si bridges, and it is essential to notice that Brönsted acidity is affected by the dependence on the Si–O–Al bond angle and the Al/Si atomic ratio [16–18]. So far, the microstructure of the surface of aluminosilicate nanoparticles has not been well investigated yet. In order to understand the properties of these systems, one needs an accurate knowledge of their microscopic structure via computer simulation. However, due to a complex interaction in the system, our understanding of the structure and thermodynamics of liquid and amorphous aluminosilicate nanoparticles is relatively poor, especially about the temperature dependence of the surface structure and surface energy of the system. On the other hand, there are several works related to the structure and dynamics of the surfaces of other oxide nanoparticles, clusters or thin films such as Al_2O_3, SiO_2, TiO_2 and Fe_2O_3 (see, for example, in [19–22]). These calculations showed that in nanosized models the surface has structural elements such as two- or threefold coordinated Al and Si sites (i.e. Si^{II} or Al^{II} and Si^{III}) that are present in the bulk only at high temperatures, whereas on those surfaces they are found at all temperatures [20, 22]. Moreover, in those structures it is essential to notice that oxygen atoms are preferred at the surface and this oxygen excess causes Al or Si enrichment just below the surface [20, 22]. The oxygen excess and subsequent Al or Si enrichment may cause interesting features near the surface in terms of low activity catalysis [18]. Analogously, it is similar to the trend of the high dispersion of Al atoms at the surface of aluminosilicate nanoparticles [11]. Therefore, it motivates us to carry out a comprehensive study on the surface structure of liquid and amorphous aluminosilicate nanoparticles. In addition, the size and temperature effects on the surface thermodynamics or glass transition temperature were also observed and presented.

2. Calculation

In order to carry out a reliable investigation of liquid and amorphous aluminosilicate nanoparticles, the suitability of the interatomic potential for surface studies needs to be evaluated. After intensive testing, we found that Born–Mayer potentials previously used in simulations of liquid and amorphous aluminum silicates can describe well both the structure and thermodynamics of aluminosilicate nanoparticles [23]. These interatomic potentials were also successfully used in our previous works for liquid and amorphous aluminosilicates, or pure Al_2O_3 and SiO_2 [24–26]. The simulations were done for a spherical particle under non-periodic boundary conditions with different sizes ranging from 2 to 5 nm, which contain a number of atoms corresponding to the real density of the amorphous aluminum silicates, i.e. $\rho = 2.6\ \mathrm{g\ cm^{-3}}$ [27]. We used the Verlet algorithm and the MD time step is 1.6 fs. The temperature of the system was decreased linearly in time as $T = T_o - \gamma \times t$, where $\gamma = 4.375 \times 10^{13}\ \mathrm{K\ s^{-1}}$ is the cooling rate and $T_o = 7000$ K is the initial temperature. Configurations at finite temperatures have been relaxed for 50 000 MD steps before calculating the static and thermodynamic properties. Moreover, in order to calculate the coordination number distributions in aluminosilicate nanoparticles, we adopt the fixed values $R_{Al-Al} = 3.80$ Å, $R_{Al-Si} = 3.70$ Å, $R_{Si-Si} = 3.50$ Å, $R_{Al-O} = 2.60$ Å, $R_{Si-O} = 2.50$ Å and $R_{O-O} = 3.70$ Å. Here R_{ij} is the cutoff radius, which was chosen as the position of the minimum after the first peak in $g_{ij}(r)$ for the amorphous models at the ambient pressure, like those used in [23, 24]. In order to improve the statistics of the simulation, the results have been averaged over six independent runs for nanoparticles with sizes of 2, 3 and 4 nm. Due to the large number of atoms in the model with the size of 5 nm (i.e. 5071 atoms) only two runs were done for this size.

3. Results and discussions

3.1. Surface static properties

Systematic analysis of the temperature dependence of the surface structure was done in detail for the 4 nm nanoparticles. Because of the lack of long range order in the structure, it is difficult to separate the surface shell from the core of the amorphous nanoparticles compared to those for crystalline nanoparticles. In order to investigate the surface of the liquid and amorphous aluminosilicate nanoparticles, we need a criterion to decide which atoms belong to the surface area and which ones belong to the core of the nanoparticle. There is no common principle for such a choice of surface or core for amorphous substances. For amorphous SiO_2 clusters, all atoms located within 5.0 Å of the hull just touching the exterior of the droplet were defined as belonging to the surface, atoms located at a distance between 5.0 and 8.0 Å from the hull belong to the transition zone and the remaining atoms belong to the interior [20]. In contrast, for the amorphous Al_2O_3 thin film they simply used the top 1.0 or 3.0 Å layer of the amorphous thin film for surface structural studies [22]. From the structural point of view it can be considered that atoms belong to the surface if, in principle, they could not have full coordination for all atomic pairs. In contrast, atoms belong to the core if, in principle, they can have full coordination for all atomic pairs like those located in the bulk (i.e. the model with periodic boundary conditions). Therefore, for simplicity we assume that atoms located in the outer shell of the spherical nanoparticle with a thickness of 3.8 Å (i.e. the largest radius of the coordination spheres used in the system) belong to the surface and the remaining atoms belong to the core of the nanoparticle. A similar determination was suggested for SiO_2 and TiO_2 nanoparticles [28, 29].

The first quantity we would like to present here is the coordination number distribution in the surface shell, which is clearly depends on the temperature and strongly differs from those observed in the core. Table 1 shows that the mean coordination number for all atomic pairs in the surface shell is smaller than that observed in the core or in the bulk. Moreover, their temperature dependence in the surface shell and in the core is not systematic, like those found for SiO_2 and TiO_2 nanoparticles [28, 29]. We found that the core of aluminosilicate nanoparticles has a distorted tetrahedral network structure, and it is close to that observed for the bulk with the mean $Z_{Al-O} \approx 4.5$ and $Z_{Si-O} \approx 4.2$ at the low temperature of 350 K [24]. In contrast, the surface

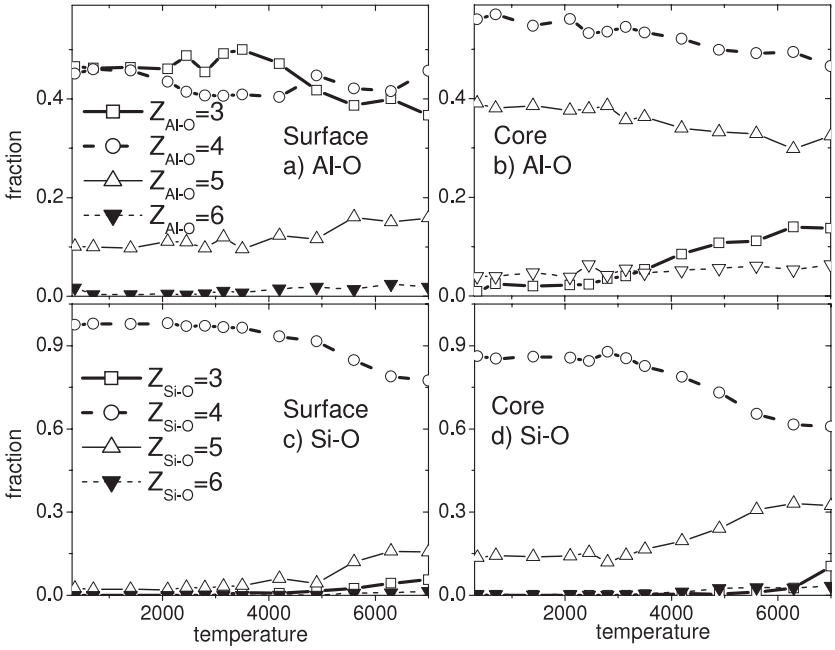

Figure 1. Coordination number distribution for Al–O and Si–O pairs upon cooling in nanoparticles with size 4 nm.

Table 1. The mean coordination number in the surface shell and in the core of nanoparticles with size 4 nm upon cooling.

T (K)		Z_{Al-Al}	Z_{Al-Si}	Z_{Si-Al}	Z_{Si-Si}	Z_{Al-O}	Z_{O-Al}	Z_{Si-O}	Z_{O-Si}	Z_{O-O}
7000	Surface	2.72	2.43	2.67	2.12	3.78	1.47	4.13	1.37	7.94
	Core	3.13	3.22	3.05	2.47	4.32	1.58	4.39	1.58	9.95
3500	Surface	2.59	2.54	2.31	2.20	3.61	1.40	4.03	1.38	7.32
	Core	4.18	2.79	3.26	2.29	4.47	1.81	4.19	1.38	9.58
2100	Surface	2.75	2.46	2.47	2.16	3.68	1.41	4.03	1.37	7.36
	Core	4.08	2.83	3.09	2.45	4.44	1.81	4.14	1.38	9.58
350	Surface	2.74	2.46	2.46	2.20	3.65	1.42	4.05	1.37	7.23
	Core	4.08	3.00	3.31	2.36	4.49	1.81	4.17	1.38	9.55
Bulk [24]		4.01	3.09	3.24	2.38	4.57	1.30	4.18	1.19	9.74

of the aluminosilicate nanoparticles has $Z_{Si-O} \approx 4.0$ and $Z_{Al-O} < 4.0$. This indicates the existence of under-coordinated structural units related to breaking bonds at the surface of the nanoparticles. Such under-coordinated structural units can be considered as structural defects, such as SiO_2, SiO_3, AlO_2, AlO_3, etc. More details about the evolution of surface structure upon cooling from the melt can be found via the changes in coordination number distributions for the Al–O and Si–O pairs. From figure 1, one can find that, upon cooling from the melt, the percentage of three-fold coordinated Al atoms to oxygen in the surface shell of the nanoparticles strongly increases at $T \geqslant 3500$ K; it then decreases slightly and reaches a value of around 46% at 350 K (i.e. it becomes the most dominant defect as there is a transition from the liquid to amorphous phase, see figure 1(a)). In addition, the fraction of Al atoms with $Z_{Al-O} = 4$ is nearly independent of temperature and it slightly decreases with decreasing temperature for $Z_{Al-O} = 5$ and $Z_{Al-O} = 6$ (see figure 1(a)). In contrast, the percentage of Si atoms with $Z_{Si-O} = 4$ increases up to about 100% at 350 K while it decreases for Si atoms with other coordination numbers (see figure 1(c)). On the other hand, we can see in figures 1(b) and (d) that AlO_4, AlO_5 and SiO_4 units are the most dominant in the core of the nanoparticles and they are the main structural units of aluminosilicate nanoparticles. This is similar to the structure of SiO_2 clusters or Al_2O_3 nanoparticles [30–32]. Additionally, due to lack of periodic order structure there is a possible large amount of another type of point defect in amorphous aluminosilicate nanoparticles, i.e. vacancy-like defects. Interstitial large pores in the surface shell of the amorphous nanoparticles can change their position with the neighboring atoms and act as vacancies in diffusion processes at high temperatures, like those found and discussed previously for amorphous Al_2O_3 [26, 33]. It seems that, due to the small dimension and specific amorphous structure, there is the existence of only typical structural point defects in the surface shells of the amorphous aluminosilicate nanoparticles just discussed. In order to get more details of structural defects in amorphous aluminosilicate nanoparticles, we focus attention on the local environment of Al and Si atoms (figure 2). One can see that, while the amorphous aluminosilicate bulk and the core of amorphous aluminosilicate nanoparticles have a distorted tetrahedral network with $Z_{Al-O} = 4.49$ and $Z_{Si-O} \approx 4.17$, the surfaces of the nanoparticles contain a significant amount of under-coordinated units of AlO_3. Therefore, the

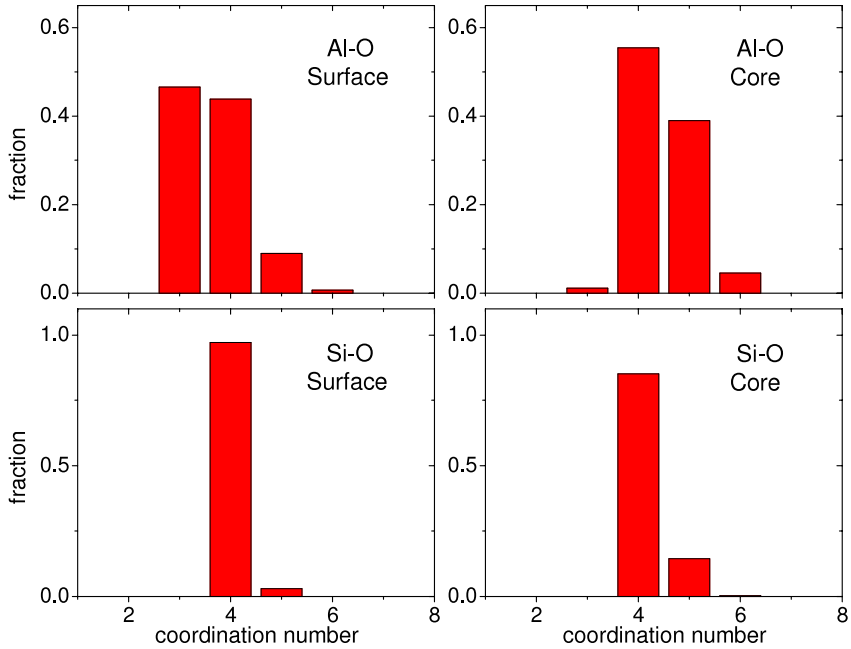

Figure 2. Coordination number distribution in amorphous aluminosilicate nanoparticles with size 4 nm at 350 K.
(This figure is in colour only in the electronic version)

mean coordination number in the surface shell for the Al–O pair is smaller, i.e. $Z_{Al-O} \approx 3.65$. Coordination number distributions for the Al–O and Si–O pairs in the surface shell and the core of the nanoparticles at 350 K were shown in figure 2. One can see that the distribution for the Si–O pair is similar in both the surface shell and the core in that Si atoms are mainly surrounded by four oxygen atoms although the fraction of SiO_5 in the core is higher than that in the former. In contrast, the distribution of the Al–O pairs in the surface shell is quite different from those observed in the core. Since Al atoms in the surface shell are mainly surrounded by three oxygen ones in addition to the fourfold-coordinated Al, one can see that Al atoms in the core are mainly surrounded by four oxygen atoms in addition to the fivefold ones. Threefold Al can be assumed as structural point defects with the oxygen deficiency [34], and as the generator of Brönsted acid sites from the silanol group when a trivalent cation, like Al^{3+}, is present in tetrahedral coordination with oxygen at the surface of the nanoparticles [18]. This result is very reasonable since the surface has more defects. Hence, one can suggest that the existence of these structural defects in the liquid and amorphous nanoparticles might enhance the diffusion of atomic species at the surface [27, 30, 35]. It might be the origin of different surface properties of aluminosilicate nanoparticles which were found experimentally in practice [15, 18]. On the other hand, structural defects in the surface shell of aluminosilicate nanoparticles may have an important role in their photoluminescence, if any, like those found for SiO_2 nanoparticles [36, 37].

In addition, we found that, upon cooling from the melt, the total number of atoms (Al, Si and O) in the core of the nanoparticles increases while it decreases in the surface shell (not shown). This phenomenon reflects the

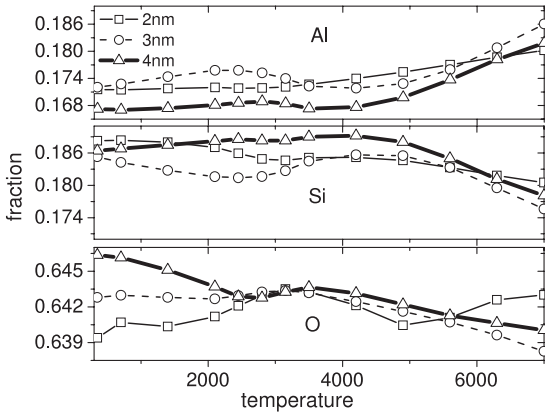

Figure 3. The ratio of the number of each atomic species per total number in the surface layer in three models upon cooling.

corresponding change not only in the mass density but also in the concentration of defects in two parts of the nanoparticles. From figure 3 one can find that, at high temperatures, Al atoms are more dominant in the surface shell than Si atoms, and their number decreases with decreasing temperature while the number of Si atoms has a tendency to increase; however, these changes are unremarkable at low temperatures. In contrast, it is significant for the number of O atoms at the surface of nanoparticles upon cooling from the melts. For sizes of 2 and 3 nm, the ratio of O atoms at the surface increases at high temperatures and then decreases on reducing to lower temperatures, i.e. $T \leqslant 3150$ K, but for size 4 nm this ratio increases with decreasing temperature. The reason for this is that, for the large amorphous aluminosilicate nanoparticle systems, it is energetically better to have an oxygen atom at the surface, since in that way only one

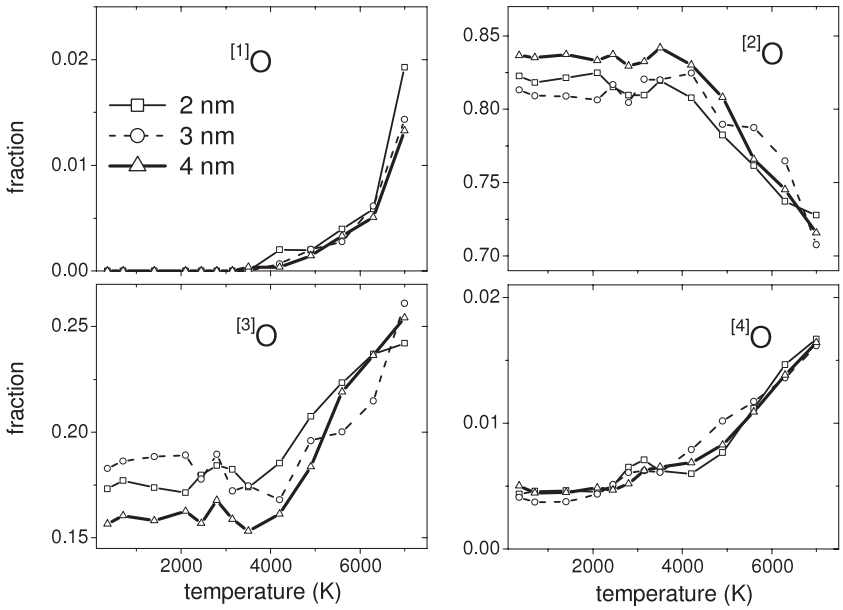

Figure 4. Number fraction of oxygen having one, two, three and four nearest T neighbors (T = Al, Si) in surface layers.

bond, if any, has to be broken (i.e. the system forms a dangling bond), whereas if an Si or Al atom is at the surface several bonds have to be broken [20, 32]. These changes involve the appearance of several vacancies on the surface and many possible arrangements of these vacancies, which not only correspond to the changes in the acidity at the surface but also to an increase of the surface area due to the reduction of alumina content in amorphous aluminosilicate nanoparticles [18, 36, 38]. Moreover, one find that at the surface layers the ratios of the number of atomic species per total number of atoms depend on the different sizes of the nanoparticles, but it is not systematic (see figure 3). It also involves the different changes of surface energies for different sizes upon cooling from the melts of nanoparticles, and more details will be shown in the next part of this paper.

On the other hand, the local environments of oxygen in aluminosilicates are also a subject of great interest [23, 27, 39–43]. It was found that there is a significant amount of $^{[2]}$O, $^{[4]}$O and $^{[5]}$O in addition to the triclusters, i.e. $^{[3]}$O, in aluminum silicate glasses [44]. Moreover, it was found clearly their role in the structure and dynamics of aluminum silicates [40–44]. Thus, it motivates us to carry out a systematic study on temperature and size dependences of the fraction of $^{[n]}$O in the liquid and amorphous aluminosilicate nanoparticles. The label $^{[n]}$O refers to the number (n) of T atoms that are nearest neighbors to a given O (i.e. T = Al, Si and $n = 0, 1, 2, 3$ or 4). Figure 4 shows the temperature dependence of fractions of $^{[1]}$O, $^{[2]}$O, $^{[3]}$O and $^{[4]}$O in nanoparticles of three sizes: 2, 3 and 4 nm. It is clear that the distributions decrease with decreasing temperature, with an exception for $^{[2]}$O in which it increases dramatically from 70% to 83% with decreasing temperature and is nearly constant for $T \leqslant 3500$ K. In contrast, the fraction of $^{[3]}$O decreases rapidly from 7000 to 3500 K and then is nearly constant with the approximate value of 17% for the three sizes. As was noticed previously in references [23, 43], SiO_5, AlO_5 and triclusters (i.e. $^{[3]}$O) facilitate the dynamics of atomic species in molten aluminum silicates [44]. Therefore, $^{[3]}$O can have an important role in the diffusion of atomic species at the surface layer of nanoparticles. Moreover, at high temperatures (i.e. at about $T \geqslant 3500$ K) non-bridging oxygen (i.e. $^{[1]}$O) also appears and its number increases with increasing temperature like those observed in the bulk [44]. Non-bridging oxygen has an important role in the diffusion of atomic species in the surface shell of nanoparticles due to their high mobility at high temperatures. In contrast, the fraction of $^{[4]}$O in the surface shell of aluminosilicate nanoparticles has a tendency to decrease with temperature and it is quite different from those observed in the bulk [44]. This result is similar to those observed in the sol–gel synthesis of a nanoparticulate aluminosilicate precursor for homogeneous mullite ceramics, and it was found that these nanoparticles have a significant amount of Al–O–Si bonds with Si atoms mostly linked to three Al^{VI} via oxygen bridges [11]. Overall, one can see that the changes in $^{[n]}$O concentration in nanoparticles with temperature, although systematic, are quite different from those observed in the bulk aluminum silicates [44].

In order to get more insights into the microstructure of the surface of aluminosilicate nanoparticles, we also present the main peaks in O–Al–O, Al–O–Al, O–Si–O and Si–O–Si bond-angle distributions. It seems that the main peaks in bond-angle distributions in the core of nanoparticles have a tendency to shift toward larger values with decreasing temperature; however, the changes are not systematic (see table 2). In contrast, no clear tendency was found for the surface (table 2). We also found that the main peak in the distribution for the O–Al–O angle in the surface shell and in the core is located at around 110° and 100°, respectively. In contrast, for the Al–O–Al angle it is located at 94° and 98° for the surface and for the core, respectively (see figures 5(a) and (b)). It is well known that, for an ideal tetrahedral network structure,

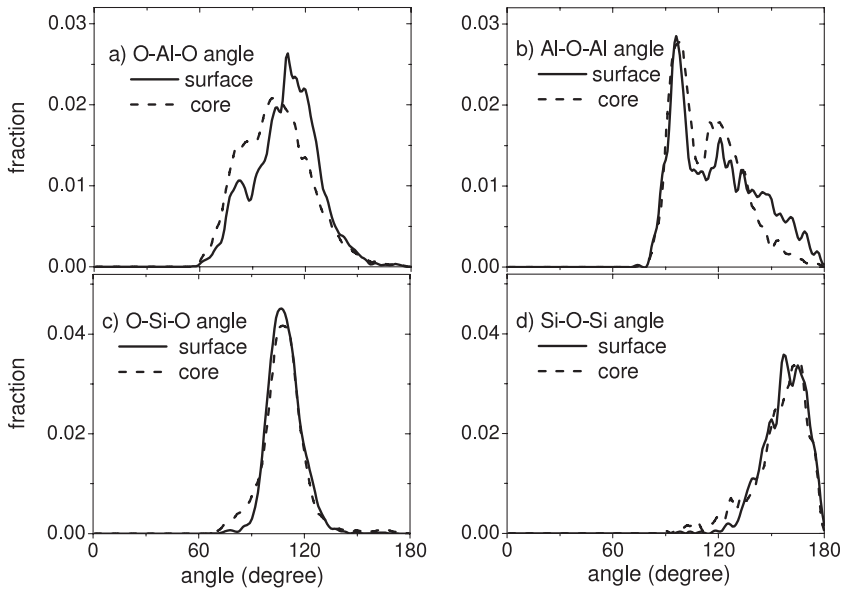

Figure 5. Bond-angle distributions in the surface of aluminosilicate nanoparticles with size 4 nm at three temperatures upon cooling compared with the average for those at 350 K.

Table 2. Mean bond angle, θ_{ijk}, in aluminosilicate nanoparticles with size 4 nm upon cooling.

T (K)		θ_{O-Al-O}	$\theta_{Al-O-Al}$	θ_{O-Si-O}	$\theta_{Si-O-Si}$
7000	Surface	95.23	103.22	108.15	138.31
	Core	89.07	98.03	95.84	148.15
3500	Surface	113.68	98.03	109.38	159.22
	Core	98.92	100.14	106.91	153.09
2100	Surface	116.14	95.23	105.71	156.78
	Core	105.71	101.41	110.01	150.01
350	Surface	110.19	96.19	106.44	157.13
	Core	100.91	97.98	105.69	162.51
Bulk [24]		99	97	108	158

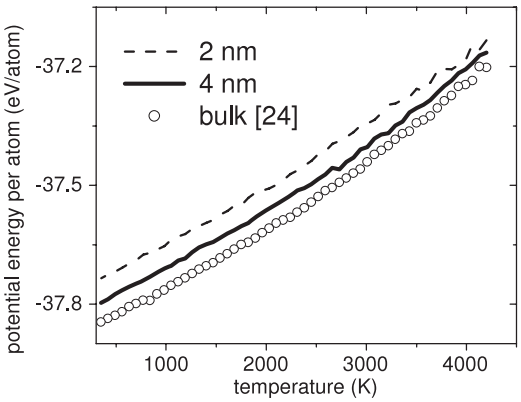

Figure 6. Temperature dependence of the potential energy of aluminosilicate nanoparticles compared with that in the bulk.

the O–Al–O angle is equal to 109.47°. The mean O–Al–O angle in the core is thus slightly smaller than that of an ideal tetrahedron due to the existence of the AlO_5 distribution. In contrast, the larger O–Al–O angle in the surface is related to the large amount of AlO_3 existing in the surface layers of the aluminosilicate nanoparticles [26]. On the other hand, one can see that the distribution for the O–Al–O angle in the core has a small peak at 84° in addition to the main peak which is located at a larger angle (figure 5(a)). From studying amorphous Al_2O_3 nanoparticles by simulations, it was found that the main peak in the O–Al–O angle distribution corresponds to the corner-sharing tetrahedra and the smaller peak corresponds to the edge-sharing tetrahedra [32]. Similarly, one can suggest that edge-sharing configurations are preferred at the surface layer of aluminosilicate nanoparticles. In contrast, the distributions for O–Si–O and Si–O–Si angles in the surface shell are very close to those in the core, it indicates the similarities of Si–O subnetworks in both parts of the nanoparticles. Figure 5(c) shows that the mean O–Si–O angle is around 105°–106° and is very close to the value 109.47° of an ideal tetrahedron [25]. The Si–O–Si angle, on the other hand, is equal to 159°–164° and is much larger than that of the Al–O–Al angle. This means that the packing of AlO_n units in the liquid and amorphous aluminosilicate nanoparticles is denser than that of SiO_n units, like that found for the bulk counterpart [23, 24]. Furthermore, the calculations show that the changes in angles at the surface and in the core upon cooling from the melt are not systematic, indicating the complicated feature of the network structure in these nanoparticles [45].

3.2. Surface energy and glass transition temperature of liquid and amorphous aluminosilicate nanoparticles

The temperature dependence of the potential energy of nanoparticles is of great interest because one can infer important quantities related to the surface energy and thermodynamics of nanoparticles from it [15, 18, 22, 46, 47]. We found the potential energy per atom, E_{pot}, and temperature dependence of E_{pot} was shown in figure 6 together with those for the bulk (i.e. amorphous aluminosilicate models

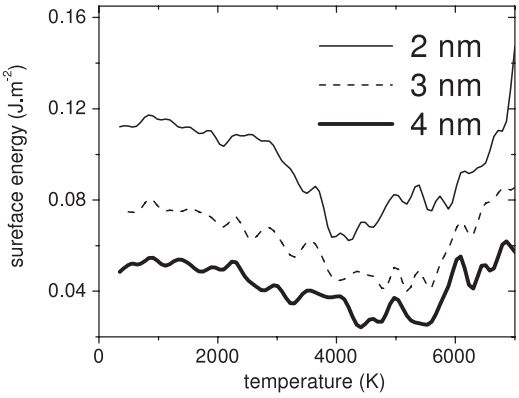

Figure 7. Temperature dependence of the surface energy for nanoparticles with different sizes.

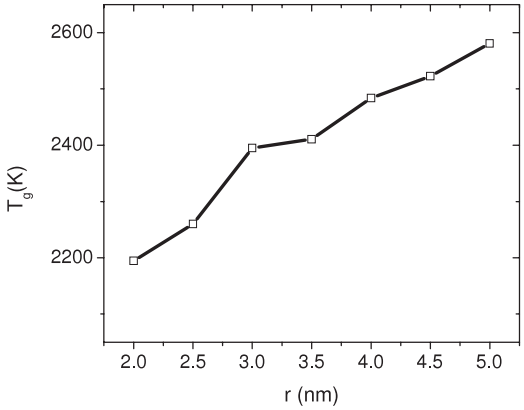

Figure 8. Size dependence of the glass transition temperature, T_g, of liquid aluminosilicate nanoparticles.

containing 3025 atoms in a cubic box under periodic boundary conditions [24]). One can see that E_{pot} for the nanoparticles is significantly higher than that for the bulk due to the surface energy of the former [20, 48]. We thus expect the relation

$$E_{pot}^{nano} - E_{pot}^{bulk} = E_s/N. \quad (1)$$

Here, E_s is the surface energy and N is the total number of atoms in the system. The most interesting observation is that the surface energy depends on the particle size over a large interval of temperature, i.e. it increases with decreasing nanoparticle size (figure 7), like that observed for silica nanoclusters with BKS interatomic potential [20]. This is, however, contrary to that observed for Lennard-Jones clusters or for silica nanoclusters [30, 49]. One can see in figure 7 that the surface energy of nanoparticles decreases with decreasing temperature, it passes through a minimum in the temperature range between 4200 and 5600 K and then it increases. The phenomenon may be related to the occurrence of a local sudden change in density of the system upon cooling from the melt, like that found for the bulk silica by using *NPT* ensemble simulation [50]. E_s has a value of around 0.02 to 0.14 J m^{-2} over the temperature range studied. There is no experimental surface energy of aluminosilicate nanoparticles to compare this with. However, an experimentally and computationally deduced value for the surface energy of amorphous silica in pure water is 0.340 J m^{-2} and in Al_2O_3 thin films it is 0.88 J m^{-2} [22, 51]. This means that the calculated E_s in the present work is quite reasonable.

The glass transition in nanoscale systems including nanoparticles, thin films and liquids in confined geometries has been under intensive investigation [52–56]. The glass transition temperature of aluminosilicate nanoparticles can be found via the intersection of a linear high-and low-temperature extrapolation of the system potential energy, like what was done for aluminum silicate liquids [23]. We found that T_g is equal to 2194.42 K, 2259.89 K, 2395.06 K, 2410.61 K, 2483.77 K, 2522.38 K and 2580.92 K for 2.0, 2.5, 3.0, 3.5, 4.0, 4.5 and 5.0 nm aluminosilicate nanoparticles, respectively. This means that T_g decreases with the reduction of nanoparticle size and is higher than that for the bulk, for which we found $T_g = 2047$ K [24] (see figure 8). A similar tendency was found for organic nanoparticles [57], however, it is contrary to that observed for liquid propylene glycol and two of its oligomers inside the pores of controlled porous glasses [58]. In order to explain the increase or decrease of T_g with the size of nanoscale substances a theoretical model based on the boundary condition dependence of T_g was proposed [59]. Our finding, furthermore, highlights the finite size effects on the glass transition which affects the stability of low-dimensional materials about it, recently found and discussed in the literature [57]. However, one can see that the finite size effects on T_g cannot be interpreted as readily as those on the melting temperature T_m due to the lack of a consensus on the nature of the glass transition [60, 61]. There were several attempts at interpretation of the finite size dependence of T_g. For example, a model of the finite size effects on T_g, borrowing ideas from the theory of the second-order phase transition, has been developed. This model predicts a downward shift and a broadening of T_g from finite size effect constraints on a correlation length defined for the glass transition [62, 63].

On the other hand, in order to study intensively the microscopic and thermodynamic properties of aluminosilicate nanoparticles, it is also necessary to have a comprehensive study of the cooling rate effects on the structure and thermodynamics of liquid and amorphous nanoparticles. Indeed, it was found that, for the bulk amorphous silica, the microscopic quantities calculated by *NPT* ensemble simulation depend significantly on the cooling rates [50]. Similar results were found for the cooling rate effects in amorphous Al_2O_3 [33, 64]. However, it was found that cooling rate effects on the static properties of monatomic amorphous nanoparticles obtained by *NVT* ensemble simulations are relatively weak while the effects on thermodynamic quantities are more pronounced [65]. It seems that similar cooling rate effects on structural properties and thermodynamic quantities in aluminosilicate nanoparticles can be suggested since we also use *NVT* ensemble simulation in the present work.

4. Conclusion

(1) Evolution of the microstructure of the surface and core of liquid and amorphous aluminosilicate nanoparticles

upon cooling from the melts has been found. It was found that the core of the amorphous nanoparticles has a distorted tetrahedral network structure with the mean $Z_{Al-O} \approx 4.5$ and $Z_{Si-O} \approx 4.2$ like that of the bulk. In contrast, the surface of the nanoparticles has a significant amount of structural defects with the mean $Z_{Al-O} < 4.0$ and $Z_{Si-O} \approx 4.0$. These defects can affect strongly the dynamics and surface properties of the amorphous aluminosilicate nanoparticles.

(2) On the other hand, upon cooling from the melts we found that the number of atoms at the surface decreases with decreasing temperature, the reduction of alumina content corresponding to changes in the properties at the surface of the aluminosilicate nanoparticles such as the acidity or the surface area. Moreover, the temperature dependence of the local environments of oxygen in aluminosilicate nanoparticles was also found, and it has been proved to have a significant role in the thermodynamics of the system at high temperatures (i.e. $T \geqslant 3500$ K).

(3) The temperature dependence of the surface energy of aluminosilicate nanoparticles was also calculated. It has been shown to have a local minimum around 4500 K which may be related to the sudden change in the density of aluminosilicate nanoparticles upon cooling from the melt. Furthermore, we also found that the glass transition temperature of aluminosilicate nanoparticles is size-dependent, in that it reduces with decreasing nanoparticle size, like observed experimentally for organic nanoparticles.

Acknowledgments

This work was supported by the Ministry of Science and Technology of HoChiMinh City, Vietnam. We gratefully acknowledge the use of the computational center of the Institute of Technology of HoChiMinh City, Vietnam.

References

[1] Schneider H, Okada K and Pask J 1994 *Mullite and Mullite Ceramics* (Chichester: Wiley)
[2] Nishio T and Fujiki Y 1991 *J. Ceram. Soc. Japan. Int. Edn* **99** 638
[3] Nishio T, Kijima K, Kajiwara K and Fujiki Y 1994 *J. Ceram. Soc. Japan. Int. Edn* **102** 464
[4] Okada K, Yasohama S, Hayashi S and Yasumori A 1998 *J. Eur. Ceram. Soc.* **18** 1879
[5] Song K C 1998 *Mater. Lett.* **35** 290
[6] Gavilan E, Doussineau T, Mansouri A E, Smaïhi M, Balme S and Janot J M 2004 *C. R. Chim.* **8** 1946
[7] Sakamoto A, Sato F and Yamamoto S 2006 *J. Non-Cryst. Solid* **352** 514
[8] Došová B, Grygar T, Martaus A, Fuitová L, Koloušek D and Machovič V 2006 *J. Colloid Interface Sci.* **302** 424
[9] Liu Y and Pinnavaia T J 2003 *J. Am. Chem. Soc.* **125** 2376
[10] Triantafyllidis K S, Lappas A A, Vasalos I A, Liu Y, Wang H and Pinnavaia T J 2006 *Catal. Today* **112** 33
[11] Leivo J, Lindén M, Teixeira C V, Puputti J, Rosenholm J, Levänen E and Mäntylä T A 2006 *J. Mater. Res.* **21** 1279
[12] Zha C and Atkins G R 2000 *J. Sol-Gel Sci. Technol.* **19** 741
[13] Tang Y F, Ling Z D, Lu Y N, Li A D, Ling H Q, Wang Y J and Shao Q Y 2002 *Mater. Chem. Phys.* **75** 265
[14] Kramer G J, de Man A J M and van Saten R A 1991 *J. Am. Chem. Soc.* **13** 6435
[15] Kuroda Y, Mori T and Yoshikawa Y 2001 *Chem. Commun.* **11** 1006
[16] O'Malley P J and Dwyer J 1988 *J. Phys. Chem.* **92** 3005
[17] Sastre G, Fornes V and Corma A 2000 *J. Phys. Chem.* B **104** 4349
[18] Parola V L, Deganello G, Scirè S and Venezia A M 2003 *J. Solid State Chem.* **174** 482
[19] Oliver P M, Watson G W, Kelsey E T and Parker S C 1997 *J. Mater. Chem.* **7** 563
[20] Roder A, Kob W and Binder K 2001 *J. Chem. Phys.* **114** 7602
[21] Baetzold R C and Yang H 2003 *J. Phys. Chem.* B **107** 14357
[22] Adiga S P, Zapol P and Curtiss L A 2003 *Phys. Rev.* B **74** 064204
[23] Hoang V V 2007 *Phys. Rev.* B **75** 174202
[24] Hoang V V, Linh N N and Hung N H 2007 *Eur. Phys. J.: Appl. Phys.* **37** 111
[25] Hoang V V, Belashchenko D K and Thuan V T M 2004 *Physica* B **348** 249
[26] Hoang V V 2004 *Phys. Rev.* B **70** 134204
[27] Winkler A, Horbach J, Kob W and Binder K 2004 *J. Chem. Phys.* **120** 384
[28] Hoang V V 2007 *J. Phys. Chem.* B **111** 12649
[29] Hoang V V 2008 *Nanotechnology* **19** 105706
[30] Schweigert I V, Lehtinen K E J, Carrier M J and Zachariah M R 2002 *Phys. Rev.* B **65** 235410
[31] Song J and Choi M 2002 *Phys. Rev.* **65** 241302
[32] Campbell T, Kalia R K, Nakano A, Vashishta P, Ogata S and Rodgers S 1999 *Phys. Rev. Lett.* **82** 4866
[33] Hoang V V 2006 *New Developments in Condensed Matter Physics* (New York: Nova Science Publisher)
[34] Diebold U 2003 *Surf. Sci. Rep.* **48** 53
[35] Litton D A and Garofalini S H 1997 *J. Non-Cryst. Solids* **217** 250
[36] Colder A, Huisken F, Trave E, Ledoux G, Guillois O, Reynaud C, Hofmeister H and Pippel E 2004 *Nanotechnology* **15** L1
[37] Stesmans A, Clemer K and Afanas'es V V 2005 *J. Phys.: Condens. Matter* **17** L393
[38] Bandosz T J, Lin C and Ritter J A 1998 *J. Colloid Interface Sci.* **198** 374
[39] Stebbins J F and Xu Z 1997 *Nature* **390** 60
[40] Morgan N A and Spera F J 1998 *Am. Mineral.* **83** 1220
[41] Bryce J G, Spera F J and Stein D J 1999 *Am. Mineral.* **84** 345
[42] Morgan N A and Spera F J 2001 *Am. Mineral.* **86** 915
[43] Pfleiderer P, Horbarch J and Binder K 2006 *Chem. Geol.* **229** 186
[44] Hoang V V 2007 *Phys. Lett.* A **386** 499
[45] Linh N N and Hoang V V 2007 *Phys. Scr.* **76** 165
[46] Shibata K, Kiyoura T, Kitagawa J, Sumiyoshi T and Tanabe K 1973 *Bull. Chem. Soc. Japan.* **46** 2985
[47] Miller J B and Ko I E 1997 *Catal. Today* **35** 269
[48] Hoang V V, Zung H and Trong N H B 2007 *Eur. Phys. J.* D **44** 515
[49] Thompson S M, Gubbins K E, Walton J P R B, Chantry R A R and Rawlinson J S 1984 *J. Chem. Phys.* **81** 530
[50] Vollmayr K, Kob W and Binder K 1996 *Phys. Rev.* B **54** 15808
[51] Mizele J, Dandurand J L and Schott J 1985 *Surf. Sci.* **162** 830
[52] Ramamoorthy M, Vanderbilt D and King-Smith R D 1994 *Phys. Rev.* B **49** 16721
[53] Oliver P M, Parker S C, Purton J and Bullett D W 1994 *Sur. Sci.* B **307–309** 1200
[54] Paxton A T and Thien-Nga L 1998 *Phys. Rev.* B **57** 1579
[55] Albaret T, Finocchi F and Noguera C 1999 *Faraday Discuss. Chem. Soc.* **114** 285
[56] Zhang H and Banfield J F 1998 *J. Mater. Chem.* **8** 20173
[57] Zhang Z, Zhao M and Jiang Q 2001 *Physica* B **293** 232

[58] Schuller J, Melnichenko Y B, Richert R and Fischer E W 1994 *Phys. Rev. Lett.* **73** 2224
[59] McCoy J D and Curro J G 2002 *J. Chem. Phys.* **116** 9154
[60] Jackson C L and McKenna G B 1996 *Chem. Mater.* **8** 2128
[61] Jiang Q, Shi H X and Zhao M 1999 *J. Chem. Phys.* **111** 2176
[62] Sappelt D and Jackle J 1993 *J. Phys. A: Math. Gen.* **26** 7325
[63] Kim K and Yamamoto R 2000 *Phys. Rev.* E **61** R41
[64] Hoang V V and Oh S K 2006 *Int. J. Mod. Phys.* B **20** 947
[65] Hoang V V, Odagaki T and Engel M 2008 *Appl. Sur. Sci.* at press doi:10.1016/j.apsusc.2007.12.050